Cracking of a concrete arch dam due to seasonal temperature variations

Theme A – 14th International Benchmark Workshop on the Numerical Analysis of Dams

de-Pouplana I.[1], Gracia L.[1], Salazar F.[1] and Oñate E.[1,2]

[1]*CIMNE – Centre Internacional de Metodes Numerics en Enginyeria, Gran Capitán s/n, 08034 Barcelona, SPAIN*

[2]*Departament d'Enginyeria Civil I Ambiental (ECA), Universitat Politècnica de Catalunya (UPC), Campus Nord, Edif. C1, C. Jordi Girona, 1-3, 08034 Barcelona, SPAIN*

E-mail: ipouplana@cimne.upc.edu

ABSTRACT: A finite element thermomechanical analysis of a concrete arch dam has been carried out to predict the extent of cracking due to temperature variations. A linear elastic analysis allows us to find out the areas exceeding the tensile strength of the concrete. Then, a smeared crack approach based on a non-local damage model is used to accurately predict the pattern of the damage at the dam. Additionally, joint elements are introduced in the damaged regions of the wall to analyze the evolution of the crack aperture over the year.

1 Introduction

Dams are particularly transcendental structures, both in the engineering and the economic fields of our society. From the engineering point of view dams are, without a doubt, challenging structures, firstly because of its proportions (some are near the largest man-made structures in the world), but also because of the hazards they pose to human settlements and infrastructures in case of failure. Indeed, incidents caused by dam failures can be catastrophic if the structure is breached or significantly damaged [1].

When dams are located in cold areas of northern countries, e.g. Sweden, Norway, Finland, the large variations in temperatures between summer and winter can cause dams to be subjected to cracking [2]. It is usual to perform routine deformation and seepage monitoring in the maintenance period of a dam to anticipate any problem and permit remedial actions if needed. However, with the recent advances in computational mechanics, the engineering community is coming to an agreement on the convenience of using numerical methods in dams' analyses, as they help understand the behaviour of the structure from the design period to the end of its service life.

Thereby, in the context of the Theme A proposed by the 14th International Benchmark Workshop on the Numerical Analysis of Dams, the present work has the objective of analysing the extent of cracking on a concrete arch dam subjected to seasonal temperature variations, by means of non-linear finite element method (NLFEM). In this regard, a thermomechanical problem is solved to determine the evolution of the deformations of the dam throughout different seasons. The non-linear behaviour of the cracked dam is captured through an integral-type non-local damage model based on the regularization of the equivalent strain [3]. An additional analysis introducing joint elements in the damaged regions is performed to give a deeper insight into the effects of cracking.

The code used to solve the problem is Kratos Multiphysics, an open-source C++ FEM framework [4]. The pre and post processing of simulations have been carried out with GiD [5].

The paper is organized as follows. First, the essential theory and formulation is introduced, including the thermomechanical problem, the damage model and the interface elements used, and then the numerical model is described along with the most representative results.

2 Formulation

2.1 Thermomechanical problem

In this work, a classical 3D solids finite element code has been coupled with the diffusion equation for the solution of a heat transfer problem. Two main equations describe the solution of the thermomechanical problem. The thermal part is governed by the heat equation:

$$\rho C \frac{\partial \theta}{\partial t} = \nabla \cdot (k \nabla \theta) + Q \tag{1}$$

where ρ is the density, C is the specific heat, θ is the temperature, k is the conductivity, and Q is the source heat. The mechanical part is governed by the balance of momentum equation:

$$\frac{\partial \sigma_{ij}}{\partial x_j} + \rho b_i = \rho \ddot{u}_i \tag{2}$$

with σ_{ij} being the stress tensor, b_i the mass forces vector, and $\ddot{u}_i$ the acceleration vector.
In this case, since the deformation of the solid part is small with respect to the scale of the problem, a one-way coupling between the thermal and the mechanical part is enough to properly capture the damage process involved in the problem of interest. In essence, the thermal problem influences the mechanical solution of the problem, but that mechanical solution takes no part in the thermal problem. Thereby, we first obtain the temperature field through all the domain by solving a diffusion problem, and then we introduce those results into the constitutive model of the solid, which act as an external load for the mechanical problem. The constitutive relation between stresses and strains can be written as:

$$\sigma_{ij} = D_{ijkl} \varepsilon_{kl} - \beta_{ij} (\theta - \theta_0) \tag{3}$$

where D_{ijkl} is the constitutive tensor of the material, ε_{kl} is the deformation tensor, β_{ij} is the thermal expansion tensor, and θ_0 is the reference temperature of the structure.

2.2 Damage model

In order to analyse the effects of the cracking on a concrete dam, different approaches can be encountered in the literature, but probably two main groups can be distinguished: the smeared crack approaches, continuum based methods in which the influence of developing fractures is incorporated into the constitutive stress-strain law [6], and the discrete crack models, in which each single discontinuity is represented explicitly [7]. In this work, we have essentially followed the smeared crack approach based on damage theory, but we have also solved the problem with joint elements, as explained in the next section.
The simplest damage model for multiaxial stress states is the isotropic damage model with a simple scalar variable. This model is based on the assumptions that the stiffness degradation is isotropic and the Poisson's ratio is not affected by damage. The stress-strain law is now postulated as:

$$\sigma_{ij} = (1 - d) D^u_{ijkl} \varepsilon_{kl} = (1 - d) \sigma^u_{ij} \tag{4}$$

where D^u_{ijkl} is the elastic constitutive tensor, σ^u_{ij} is the undamaged stress tensor, and d is the damage variable, a scalar measure of the material degradation that ranges from 0 to 1.
In order to properly determine the evolution of the damage variable regardless of the loading case we must introduce a historical variable r(t):

$$r(t) = \max \left\{ r_y, \max_{\tau \leq t} \varepsilon_{eq}(\tau) \right\} \tag{5}$$

In the above expression ε_{eq} is the equivalent strain, i.e. a scalar measure of the strain level, and r_y is the damage threshold, a material parameter that indicates the value of equivalent strain at which damage stats.

Equivalent strain

To some extent, the equivalent strain presented in (5) plays a role similar to the yield function in plasticity, because it directly affects the shape of the elastic domain. There are numerous forms of equivalent strain in the literature, but a convenient choice for concrete is to use the so called modified von Mises definition [8]:

$$\varepsilon_{eq} = \frac{\kappa - 1}{2\kappa(1-2\nu)} I_1 + \frac{1}{2\kappa}\sqrt{\left(\frac{\kappa-1}{1-2\nu} I_1\right)^2 + \frac{12\kappa}{(1+\nu)^2} J_2} \tag{6}$$

where κ is a parameter that sets the ratio between the uniaxial compressive strength and the uniaxial tensile strength, ν is the Poisson's ratio, I_1 is the first invariant of the strain tensor, and J_2 is second invariant of the deviatoric strain tensor.

Damage evolution law

There are various damage governing laws that can be effectively used to model damage growth in quasi-brittle materials. Here we use the exponential softening model proposed in [9]:

$$g(r) = 1 - \frac{r_y(1-R)}{r} - R\exp\left\{-S\left(r - r_y\right)\right\} \tag{7}$$

In equation (7) the parameter R is associated to the residual strength of the material, whereas the parameter S controls the slope of the softening branch after the peak of the stress-strain curve.

Non-local damage

Problems involving damage progression in quasi-brittle materials show strong localization of strains. If the damage parameter depends only on the strain state at the point under consideration and no regularization is introduced, numerical simulations exhibit a pathological mesh dependence and the energy consumed by the fracture process tends to zero as the mesh is refined [10]. The introduction of a characteristic length into the constitutive model, and the formulation of a non-local strain-softening model, have been shown to prevent the spurious localization of strains and regularize the boundary value problem [11-13]. An integral-type non-local damage model has been used here to that purpose.

In essence, such model abandons the classical assumption of locality and admits that the damage at a certain point depends, not only on the state variables at that point, but also on the distribution of the state variables over a finite neighbourhood of the point under consideration. The damage in the present work has been computed from the non-local equivalent strain [5]. Let $\varepsilon_{eq,l}(\mathbf{x})$ be the local equivalent strain in a domain Ω. The corresponding non-local field is defined as:

$$\varepsilon_{eq,nl}(\boldsymbol{x}) = \int_{\Omega} \zeta(\boldsymbol{x},\boldsymbol{\chi})\,\varepsilon_{eq,l}(\boldsymbol{\chi})\,d\boldsymbol{\chi} \tag{8}$$

where $\zeta(\mathbf{x},\boldsymbol{\chi})$ is the non-local weighting function:

$$\zeta(\boldsymbol{x},\boldsymbol{\chi}) = \frac{\zeta_0(\|\boldsymbol{x}-\boldsymbol{\chi}\|)}{\int_{\Omega}\zeta_0(\|\boldsymbol{x}-\boldsymbol{\varphi}\|)d\boldsymbol{\varphi}}\,;\quad \zeta_0(\|\boldsymbol{x}-\boldsymbol{\chi}\|) = \zeta_0(D_{x\chi}) = \begin{cases} \exp\left[-\left(\dfrac{2D_{x\chi}}{l_c}\right)^2\right] & \text{if } D_{x\chi} \le l_c \\ 0 & \text{if } D_{x\chi} > l_c \end{cases} \tag{9}$$

where $D_{x\chi}$ is the distance between points **x** and **χ**, and l_c is the characteristic length of the material. The function ζ_0 in (9) implies that any point **χ** within a radius l_c of the source point **x** has an influence on the value of the non-local equivalent strain in **x**.

2.3 Joint elements

Joint elements (or interface elements) are special elements that allow representing discontinuities in the displacement field as a discrete crack model. One of the most important differences with respect to the standard finite elements is that the quantities of interest in the interface elements are in the local coordinate system of the crack. It is thus necessary to define the upper and lower faces of the joint and work with the normal and tangential relative displacements at any point along the fracture.

The constitutive law governing the mechanical behaviour of the interface element is a bilinear cohesive fracture model based on the fracture criteria of Camacho and Ortiz [14] and Song *et al.* [15]. In such model the evolution of the cohesive zone is an irreversible damage process with a historical state variable ι, playing a similar role as the scalar r defined in (5):

$$\iota(t) = \min\left\{\max\left\{\iota_y, \max_{\tau \le t} \varepsilon_{eq}(\tau)\right\}, 1\right\} \tag{10}$$

The parameter ι_y in (10) is the damage threshold of the joints and ε_{eq} is the equivalent strain, which depends on the simultaneous activation of the tangential and normal relative displacements ϵ_i (i = l,m,n):

$$\varepsilon_{eq} = \frac{\sqrt{\epsilon_l^2 + \epsilon_m^2 + \epsilon_n^2}}{\epsilon_c} \tag{11}$$

with ϵ_c being the critical displacement, i.e. the relative displacement at which the cohesive zone stops transmitting forces. We define each component of the stress vector as:

$$\sigma_i = \frac{\sigma_y (1 - \iota)}{\iota \epsilon_c \left(1 - \iota_y\right)} \epsilon_i \tag{12}$$

where σ_y is the yield stress, i.e. the stress at which the cohesive zone starts damaging.

3 Numerical model and results

In order to consider the steel reinforcement, the dam body was divided into three pieces with different material properties, according to the percentages of concrete and steel. In essence, the upstream part was defined with a 0.324% of steel, the downstream volume with a 0.487% of steel, and the middle volume was pure concrete. The material parameters used here are summarized in Table 1.

A mesh of linear tetrahedrons was used both for the thermal and mechanical analyses. An element size of 0.75m was assigned for the dam, and a transition from 0.75 to 10m was chosen for the rock. The resultant mesh has 187,021 nodes and 1,008,000 elements (Figure 1).

3.1 Thermal analysis

Two transient thermal analyses have been performed following the indications of the problem statement. A first simulation of 26 months was carried out, starting from a cold year and followed by a warm year, and then another 26-months simulation going from a warm year to a cold year was performed so as to assess the relevance of the seasons' order (Figure 2).

From the two thermal analyses it can be concluded that the order of the seasons shows no noticeable changes in the temperature distribution at the central section of the dam, and thus here we just display the temperatures of the coldest January and the hottest July of the cold-

warm analysis (Figure 3). The yearly temperature variation near the upstream face is remarkably lower due to the influence of the reservoir.

Table 1: Material properties.

Property	**Rock**	**Dam**			**Joints**	**Unit**
		Upstream	**Middle**	**Downs.**		
Density (ρ)	2.7e3	2.32e3	2.3e3	2.33e3	2.3e3	kg/m^3
Young's modulus (E)	4.0e10	3.35e10	3.3e10	3.38e10	3.3e10	N/m^2
Poisson's ratio (ν)	0.15	0.2	0.2	0.2	0.2	-
Thermal expansion (β)	1.0e-5	1.0e-5	1.0e-5	1.0e-5	-	K^{-1}
Thermal conductiv. (k)	3.0	2.12	2.0	2.18	-	W/(m*K)
Specif. heat capacity (C)	850.0	898.5	900.0	897.8	-	J/(kg*K)
Strength ratio (κ)	10.0	13.1	13.1	13.1	-	-
Residual strength (R)	0.8	0.75	0.8	0.7	-	-
Softening slope (S)	9.0e3	9.25e3	9.0e3	9.5e3	-	-
Damage threshold (r_y,t_y)	1.0e-3	2.5e-4	2.5e-4	2.5e-4	0.04	-
Min. joint width (δ_{min})	-	-	-	-	1.0e-3	m
Critical displacem. (ϵ_c)	-	-	-	-	0.05	m
Yield stress (σ_y)	-	-	-	-	0.0	N/m^2
Friction coefficient (μ)	-	-	-	-	0.4	-

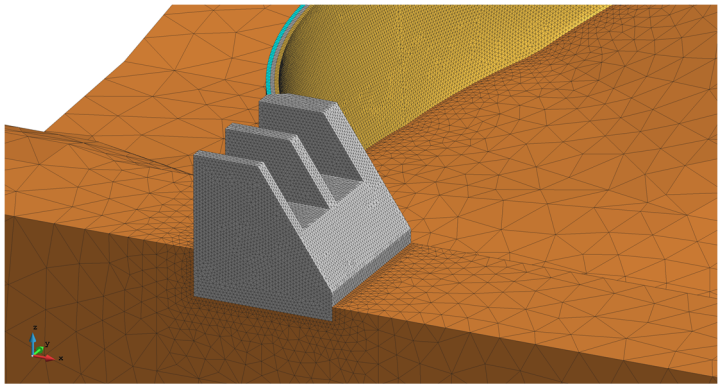

Figure 1: Detailed view of the mesh.

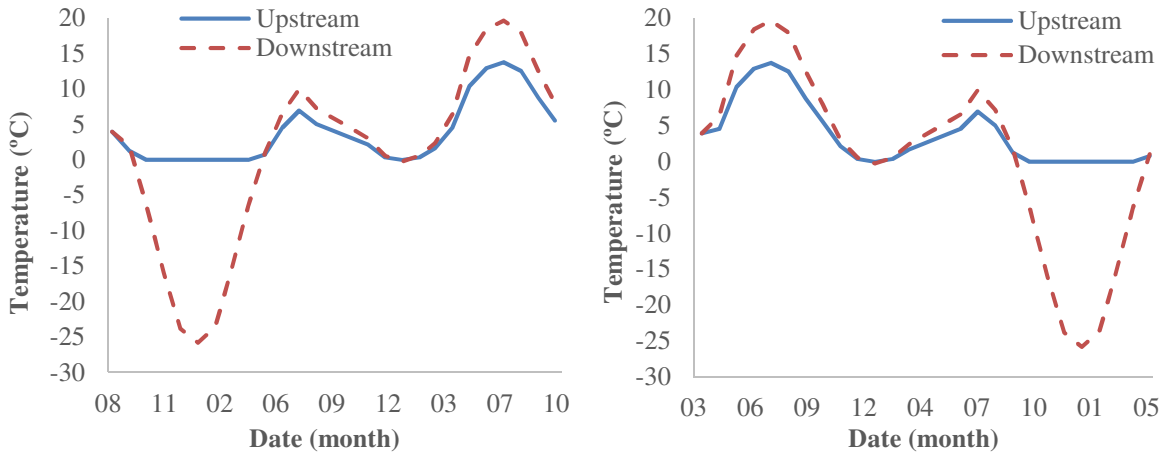

Figure 2: Temperature variation. Left: cold-warm analysis. Right: warm-cold analysis.

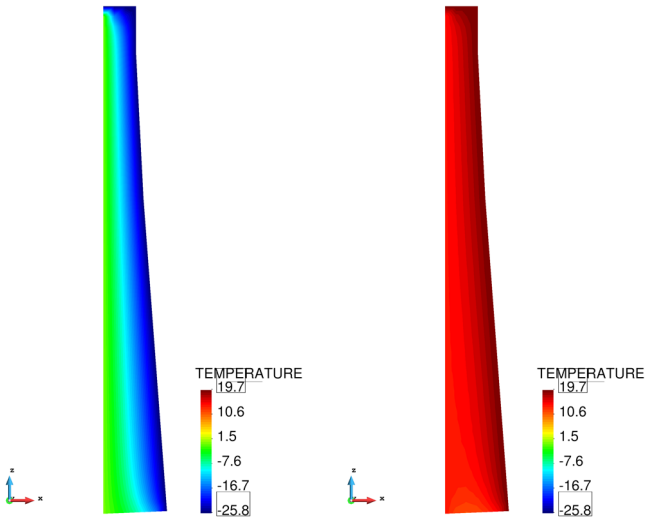

Figure 3: Temperature at the central section of the dam. Left: January. Right: July.

3.2 Linear mechanical analysis

The temperature field obtained from the thermal analysis along with the gravity load applied on the dam body and the constant hydrostatic pressure corresponding to a water level of the crest height conform the external forces applied in the mechanical analyses. An implicit and quasi-static scheme was used for this purpose.

As in the thermal analysis, the results obtained for the linear mechanical analysis of the warm-cold sequence are almost identical to those of the cold-warm alternative. Thereby, Figures 4-6 represent just the latter case.

In Figure 4, three different scenarios are plotted for each graph: static, representing a case in which no temperature variation is considered, minimum, corresponding to the hottest July of the simulation, and maximum, coinciding with the coldest January. Looking carefully at Figures 4 and 5 it is easy to understand the response of the dam against the temperature variations. While in January the wall deforms in the downstream direction, the higher temperatures on the downstream face in July induce the opposite effect. Moreover, the computed displacements near the foundation of the dam are smaller than those close to the crest given the higher stiffness of the rock mass. Also, when looking at the displacements along the horizontal lines of the arch, one also notices the influence of the abutments and the spillway.

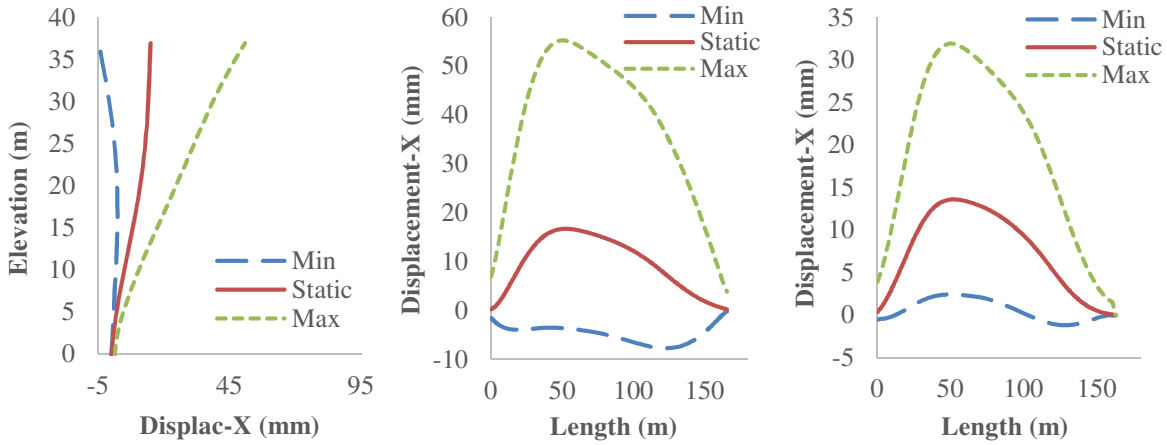

Figure 4: Displacement-X at the downstream face of the dam. Left: central section. Centre: crest. Right: 14 m below crest.

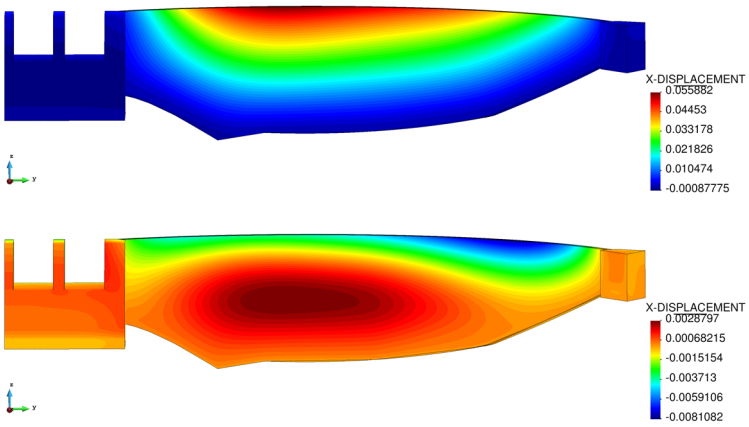

Figure 5: Contour plots of the Displacement-X. Top: January. Bottom: July.

Figure 6 displays those areas exceeding the tensile strength (2.9e6 Pa), and shows that all the downstream face can be seriously damaged by the cold temperatures of January. Looking at the main wall, one can foresee three specific regions of potential cracking: one next to the left abutment, another near the spillway, and finally one at the centre, coinciding with a sudden change of slope at the dam foundation.

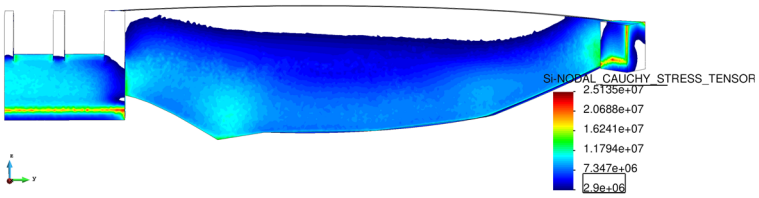

Figure 6: Contour plots of the principal stresses exceeding the tensile strength (January).

3.3 Non-linear mechanical analysis

Next, the same problem has been solved with the non-local damage model presented in the previous section using a characteristic length l_c of 1.5 m. In this case, though, some differences were found between the warm-cold (W-C) and cold-warm (C-W) sequences, stressing the higher complexity of the non-linear analysis.

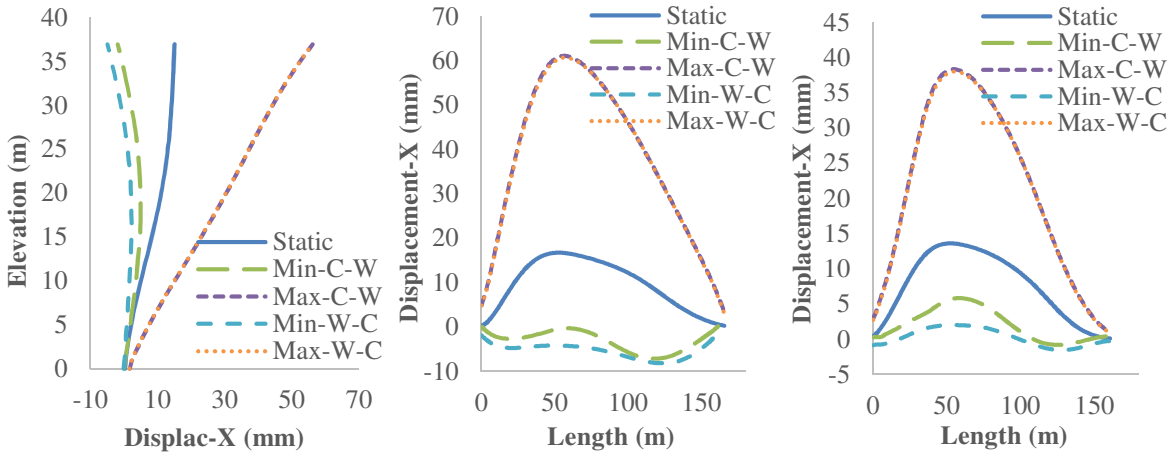

Figure 7: Displacement-X at the downstream face of the dam. Left: central section. Centre: crest. Right: 14 m below crest.

Figures 7 and 8 clearly show the previous statement. In essence, since temperatures in the warm year are smoother than those in the cold year, the sequence warm-cold shows almost no damage until the second half of the simulation. In the opposite sequence, the damage appears in the first months and thus the minimum displacement, i.e. that corresponding to the hottest month, is clearly influenced by the presence of damage at the wall. On the other hand, the difference in the computed displacement disappears in the coldest month of the year because that is the moment in which damage actually spreads for both sequences.

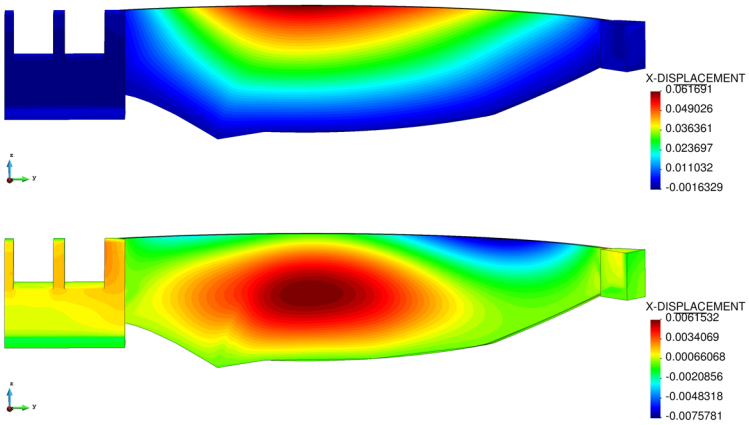

Figure 8: Contour plots of the Displacement-X. Top: January. Bottom: July.

Looking now at Figure 9 and comparing it with Figure 6, it is easy to make a correlation between the areas exceeding the tensile strength and the extent of the damage variable. Indeed, one can see that the downstream face is extensively damaged and, regarding the main wall, the damage concentrates in the same three regions of Figure 6: near the abutment and the spillway, and over the lowest point of the foundation.
Knowing the damage pattern of Figure 9, it is very straightforward to understand the displacement field of Figure 8. The contour plot is very similar to the one in Figure 5 with the exception of a smooth jump in the displacement near the central crack of the wall.

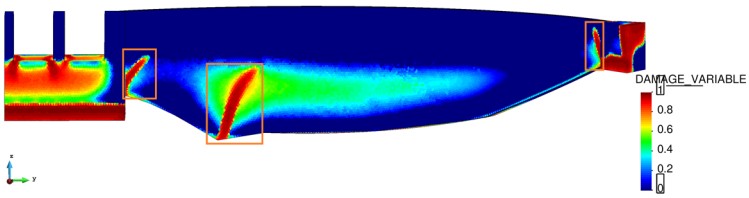

Figure 9: Contour plots of the damage variable at the end of the cold-warm analysis.

3.4 Mechanical analysis using joint elements

As an additional simulation, we have introduced joint elements to explicitly represent the cracks at the location of the three damage marks in Figure 9, and we have solved the problem defining the materials of the dam as linear elastic. The parameters of the joints are listed in Table 1.
The main purpose of this last case was to compare the effect of the joints with the non-local damage model of section 3.3. Looking at Figure 10, one can see that the joint elements, as a discrete crack approach, introduce a more abrupt jump in the displacement field than the smeared crack model based on damage. The contour plot displayed here is very similar to the one in Figure 5 because the materials are considered elastic in both cases. A combination of the

damage model with the discrete crack approach is also possible, but the computational cost would have been considerably higher.

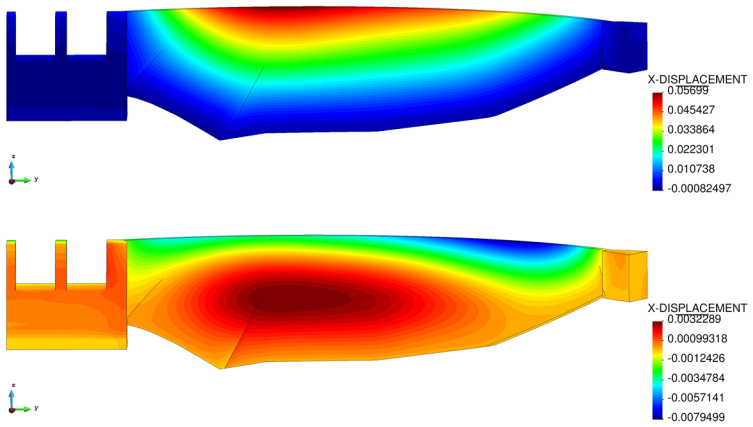

Figure 10: Contour plots of the Displacement-X. Top: January. Bottom: July.

Finally, we have also measured the crack aperture throughout the 26 months of simulation to check the influence of the seasonal temperatures on it (Figure 11). As expected, the joints open in winter when the dam is contracted, and remain almost closed during the rest of the year. It is interesting to note that, after a cold year, the width of the joints in the warm year is larger than in the opposite sequence of seasons.

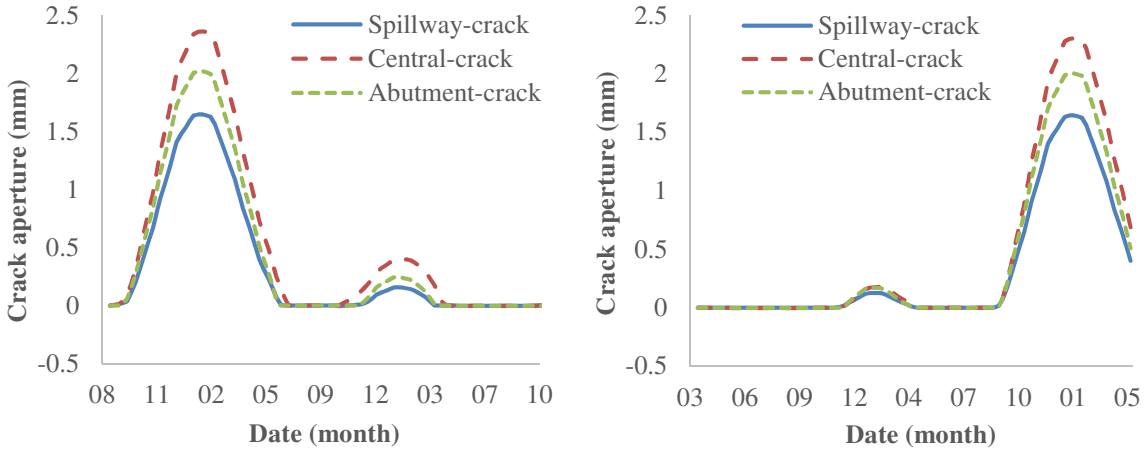

Figure 11: Crack aperture. Left: cold-warm analysis. Right: warm-cold analysis.

4 Conclusions

A non-linear finite element thermomechanical analysis of a concrete arch dam has been performed with the following conclusions:

- Temperature variations can cause important cracking on the dam, both at the abutments and at the main wall.
- A linear elastic analysis can be adequately used to predict areas that may be subjected to cracking with a relatively low computational cost.
- A non-local damage method has been used to accurately locate the regions of concentrated cracking at the wall of the dam. Moreover, it has also shown that the order of seasonal temperatures is relevant in the final prediction of deformations.

- While the smeared crack approach is very useful in the prediction of the location of cracks, it gives no information on the width of the cracks over the year. Using a discrete crack approach, such as the joint elements presented here, allows measuring the evolution of the joint aperture, which strongly depends on the temperature seasonal variations.

In the authors' opinion, the numerical tools used in the present work can be effectively used to predict and analyse the source of problems in concrete arch dams subjected to temperature variations. However, it is undoubtedly crucial to calibrate the results with real measurements in order to give a convincing message to the industry.

5 Acknowledgements

We acknowledge the financial support to CIMNE via the CERCA Programme / Generalitat de Catalunya. The research was also supported by the Spanish Ministry of Economy and Competitiveness (Ministerio de Economía y Competitividad, MINECO) through the projects ACOMBO (RTC-2015-3794-5) and NUMA (RTC-2016-4859-5).

6 References

[1] Seed H. B. and Duncan J. M. (1981, June). The Teton dam failure–a retrospective review. In Soil mechanics and foundation engineering: proceedings of the 10th international conference on soil mechanics and foundation engineering, Stockholm (pp. 15-19).

[2] Malm R. and Ansell A. (2011) *Cracking of Concrete Buttress Dam Due to Seasonal Temperature Variation.* ACI Structural Journal, 108-S02, pp, 13-22.

[3] Bazant Z. P. and Jirásek M. (2002) Nonlocal integral formulations of plasticity and damage: survey of progress. Journal of Engineering Mechanics, 128(11):1119–1149.

[4] Kratos Multiphyisics. http://www.cimne.com/kratos/, June 2017.

[5] GiD the personal pre and post processor. http://www.gidhome.com/, June 2017.

[6] Lubliner J., Oliver J., Oller S. and Oñate E. (1989) A plastic-damage model for concrete. International Journal of Solids and Structures, 25(3):299–326.

[7] Etse G., Caggiano A. and Vrech S. (2012) Multiscale failure analysis of fiber reinforced concrete based on a discrete crack model. International journal of fracture, 178(1-2):131–146.

[8] De Vree J., Brekelmans W. and Van Gils M. (1995) Comparison of nonlocal approaches in continuum damage mechanics. Computers & Structures, 55(4):581–588.

[9] Mazars J. (1986) A description of micro-and macroscale damage of concrete structures. Engineering Fracture Mechanics, 25(5):729–737.

[10] Bazant Z. P., Belytschko T. B. and Chang T.-P. (1984) Continuum theory for strainsoftening. Journal of Engineering Mechanics, 110(12):1666–1692.

[11] Eringen A. C. (1981) On nonlocal plasticity. International Journal of Engineering Science, 19(12):1461–1474.

[12] Pijaudier-Cabot G. and Bazant Z. P. (1987) Nonlocal damage theory. Journal of Engineering Mechanics, 113(10):1512–1533.

[13] Rodríguez-Ferran A., Morata I. and Huerta A. (2005) A new damage model based on non-local displacements. International Journal for Numerical and Analytical Methods in Geomechanics, 29(5):473–493.

[14] Camacho G. T. and Ortiz M. (1996) Computational modelling of impact damage in brittle materials. International Journal of Solids and Structures, 33(20):2899–2938.

[15] Song S. H., Paulino G. H. and Buttlar W. G. (2006) A bilinear cohesive zone model tailored for fracture of asphalt concrete considering viscoelastic bulk material. Engineering Fracture Mechanics, 73(18):2829–2848.